



CHORUS

This is the accepted manuscript made available via CHORUS. The article has been published as:

Laser-spectroscopy measurement of the fine-structure splitting $2^{\{3\}}P_{\{1\}}-2^{\{3\}}P_{\{2\}}$ of $^{\{4\}}\text{He}$

G.-P. Feng, X. Zheng, Y. R. Sun, and S.-M. Hu

Phys. Rev. A **91**, 030502 — Published 23 March 2015

DOI: [10.1103/PhysRevA.91.030502](https://doi.org/10.1103/PhysRevA.91.030502)

Laser spectroscopy measurement of the fine structure splitting 2^3P_1 - 2^3P_2 of ^4He

G.-P. Feng[†], X. Zheng[†], Y. R. Sun^{*}, S.-M. Hu

Hefei National Laboratory for Physical Sciences at the Microscale, Collaborative
Innovation Center of Chemistry for Energy Materials, University of Science and Technology of China,
Hefei, 230026 China

Abstract

Laser spectroscopy has been performed on a beam of neutral ^4He atoms. By using transverse laser cooling and focusing, we are able to prepare a bright beam of atoms in the metastable state 2^3S_1 deflected from the original effusive atomic beam. The initial state preparation is completed with optical pumping on the $2^3P_1 \leftarrow 2^3S_1$ transition at the wavelength of 1083 nm, followed by laser spectroscopy on the $2^3P_{1,2} \leftarrow 2^3S_1$ transitions. The 2^3P_1 - 2^3P_2 fine structure splitting is determined to be $2\,291\,177.69 \pm 0.36$ kHz. The quantum interference effect is included in data extraction. This is the most precise laser spectroscopy measurement of the interval. Our result is in agreement with both the latest QED-based calculation and the most precise measurement conducted with microwave spectroscopy.

Introduction

The neutral helium is a precisely calculable bound-state quantum system. Its fine structure, in particular the splitting intervals among the 2^3P_J ($J = 0, 1, 2$) levels, has been of great interest for verifying theoretical calculations including high-order quantum electrodynamic (QED) effects [1-3] and for the determination of the fine structure constant α [4, 5]. The larger interval in the 2^3P_J manifold, $\nu_{01} = \nu(2^3P_0) - \nu(2^3P_1) \approx 29.6$ GHz, is more suitable for the determination of α , while the smaller one, $\nu_{12} = \nu(2^3P_1) - \nu(2^3P_2) \approx 2.29$ GHz, is particularly useful to test the atomic structure calculations [6]. Over the past two decades, there have been a series of experimental investigations on the 2^3P_J fine structure splitting, and results with uncertainties below 1 kHz have been reported recently [7-13]. In parallel to the experimental effort, over the past fifty years, the theorists gradually included all the terms up to the order of $\alpha^5\text{Ry}$ (Ry is the Rydberg constant) in their calculations (see Ref. [6] and references therein). Calculated values of ν_{01} and ν_{12} have been reported with sub-kHz uncertainties [6, 14], but the deviations were as large as 10 kHz. Significant disagreement between the calculations and the measurements by as much as 36σ (16 kHz) had existed until the latest theoretical work by Pachucki *et al.* [3] which gave an uncertainty of 1.7 kHz. Moreover, as shown in Fig. 1, there are also disagreements among the most precise measurements of the 2^3P_1 - 2^3P_2 interval employing different methods, including laser spectroscopy in an atomic beam (North Texas '00) [7], saturation laser spectroscopy in a gas cell (Harvard '05) [11], and microwave spectroscopy (York '09) [12]. Marsman *et al.*

[†] Authors equally contributed to this work.

^{*} To whom correspondence should be addressed: robert@mail.ustc.edu.cn (Y. R. Sun)

proposed that a major source of the discrepancy was the effect of quantum interference among the 2^3P_j levels. [15] By correcting for this effect the published results of North Texas '00 [7], its value shifted towards and now agrees with that of York '09 [12]. Due to the complexity of saturation spectroscopy, a similar correction has not been applied to Harvard '05 [11], therefore the discrepancy has not yet been fully solved. In view of the important role that this interval has played in the parallel efforts in both theory and experiment, additional measurements and, indeed, calculations are helpful.

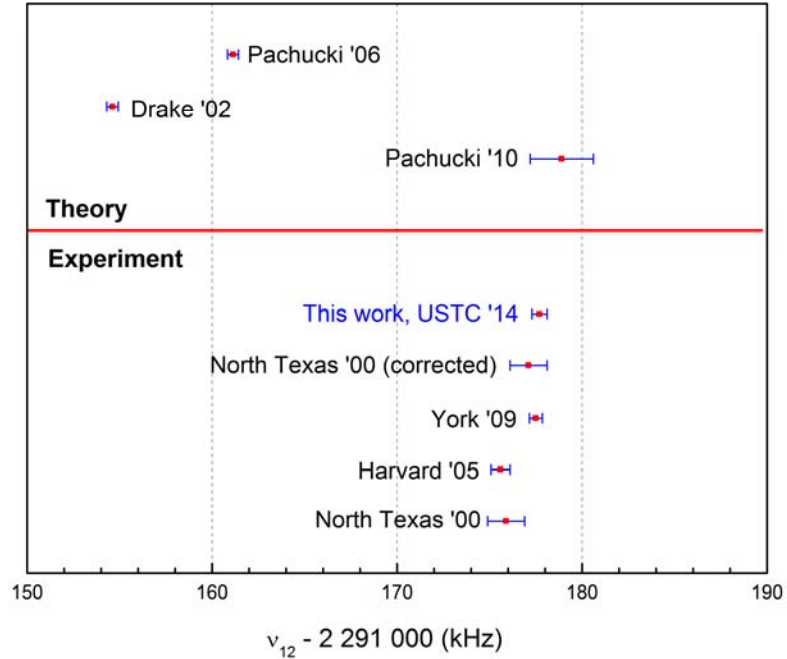


Fig. 1 (Color online) Comparison of the ν_{12} values from experimental and theoretical studies.

In this work, we study the fine structure of ^4He by performing laser spectroscopy on a state-selected helium atomic beam. Transverse laser cooling and optical pumping are used to produce an intense atomic beam of helium in a single spin state of the metastable 2^3S_1 . The spectral probing is accomplished in a well-shielded space, isolated from the noise of the surrounding electric, magnetic, and optical fields. The 2^3P_1 - 2^3P_2 interval is determined from the difference of the frequencies of the $2^3P_1 \leftarrow 2^3S_1$ and $2^3P_2 \leftarrow 2^3S_1$. This work represents the most precise laser spectroscopy measurement of the interval. Its result is in agreement with both the latest QED-based calculation Pachucki '10 [3] and the most precise measurement conducted with microwave spectroscopy York '09 [12]. It also agrees well with the corrected laser spectroscopy measurement North Texas '00 [7, 15].

Experimental setup

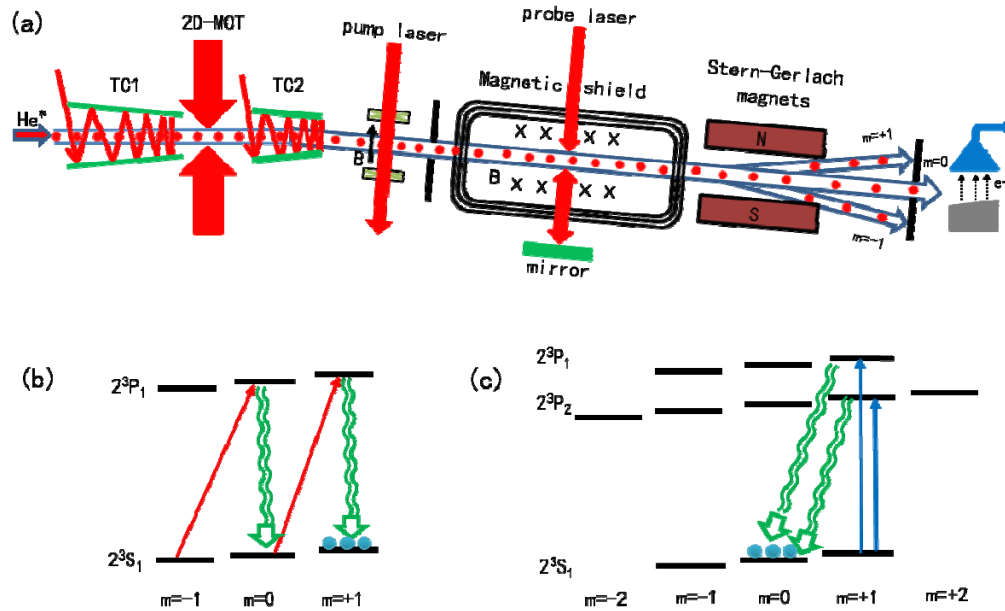


Fig.2 (Color online) Configurations of the experimental setup (a) and the schemes for optical pumping (b) and spectral excitation (c).

The schematic of the experiment is shown in Fig.2(a). An atomic beam of helium in the metastable $2S$ states is produced by a radio-frequency (rf) driven gas discharge [16] and cooled to the liquid nitrogen temperature. While both the 2^1S_0 and 2^3S_1 metastable states are populated, only atoms in 2^3S_1 are transversely cooled and focused by 1083 nm laser beams near the resonance of $2^3P_2 \leftarrow 2^3S_1$. A transversely directed, two-dimensional magneto-optical trap (2D-MOT) slightly focuses the atomic beam. The combination of the 2D transvers-cooling (TC1) and 2D-MOT enhances the intensity of the atomic beam (in 2^3S_1) by a factor of 50 in the detecting region 3 meters downstream from the discharge. [17] A second transvers-cooling region (TC2) deflects the already collimated atomic beam in the 2^3S_1 state from the original atomic beam spread by an angle of about 0.14° . Narrow collimation slits are installed along the beamline so that only the deflected atoms in 2^3S_1 are allowed to reach the detector. Compared to the previous methods of using either a strong electric field or a bright lamp to selectively quench the helium atoms in 2^1S_0 , the present method has the advantage of also blocking out the UV photons from the discharge source.

At the detection end, the metastable atoms pass through a Stern-Gerlach magnet for spin-state selection. The permanent magnet setup is 30 cm long along the direction of the atomic beam, and produces a vertical field gradient of about 0.5 T/cm. Those 2^3S_1 atoms in the $m = \pm 1$ states are deflected by the magnet; only the atoms in the $m = 0$ state reach the metastable atom detector: upon hitting a polished stainless-steel plate, the metastable atom ejects electrons, which are detected by a channeltron (Photonics CEM4920).

In the middle section of the apparatus devoted to optical pumping, a σ^+ circularly polarized laser beam from a distributed feedback laser, here referred to as the “pump laser”, is

applied to resonantly excite the atoms on the $2^3S_1 \rightarrow 2^3P_1$ transition, and clear the atomic population from the $2^3S_1 m=0$ state (Fig. 2b). Following less than 20 cycles of excitation and spontaneous decay, over 99% of the atoms are transferred to the $2^3S_1 m = +1$ state (or the $m = -1$ state when the polarization of the pump laser is switched to σ^-).

The optically pumped atoms then enter the spectral probe zone inside three layers of cylinder-shaped μ -metal shields. The residual magnetic field near the center is less than 0.5mG. An external-cavity diode laser is used for spectral scan and probing (referred to as the “probe laser”). The probe laser repopulates the $2^3S_1, m = 0$ state by exciting either the $2^3P_2 \leftarrow 2^3S_1$ or $2^3P_1 \leftarrow 2^3S_1$ transition (Fig. 2c), resulting in a signal in the channeltron detector downstream. The frequency of the probe laser is locked to a longitudinal mode of a temperature-stabilized Fabry-Pérot cavity made of ultra-low expansion glass [18, 19]. A fiber electro-optic modulator (EOM) is used to produce tunable sidebands for spectral scanning. The EOM is driven by a radio-frequency (rf) synthesizer (Agilent N9310A) referenced to the GPS signal (Spectratime GPS Reference-2000). Each set of frequency scans (Fig. 3) cover both the $2^3P_2 \leftarrow 2^3S_1$ and $2^3P_1 \leftarrow 2^3S_1$ transitions, with altogether 44 frequency points around both peaks. The scan sequence is purposely set random to avoid possible systematic shift due to frequency drifts.

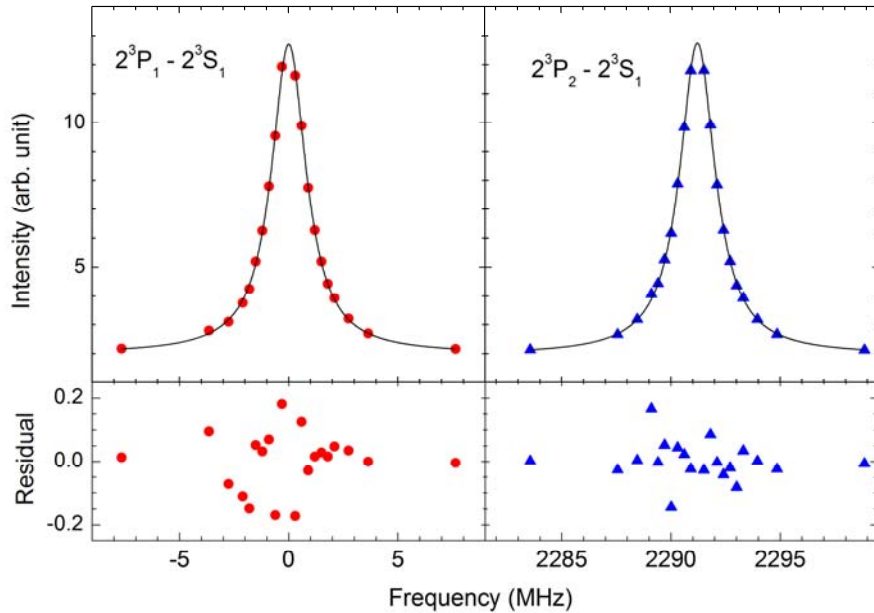


Fig. 3 (Color online) Spectrum of the $2^3P_1 \leftarrow 2^3S_1$ and $2^3P_2 \leftarrow 2^3S_1$ transitions obtained from a single scan. The scattered points are experimental data and the continuous curve is the simulated spectrum. The deviations between experimental and simulated spectra are shown in the lower panels.

Results and discussions

Various systematic effects have been studied and are described in the following.

Power Dependence: Here we study the dependence of the measured frequency interval on the power of the probing laser beam due to effects including the AC Stark shift. Under each experimental condition, a series of measurements were carried out with varying power levels for the probe laser beam. The maximum applied power was below 1/3 of the saturation power of the studied transition. Corresponding values at the zero-power limit were extrapolated. We also did the measurements both with and without a retro-reflected probe laser beam in order to investigate the degree to which the Doppler shift is cancelled. As shown in Fig.4, for measurements based on the same polarization ($m = +1$ or $m = -1$), which were taken with other experimental conditions unchanged, the extrapolations to the zero-power limit, both the non-reflected and retro-reflected, agrees with each other within the statistical uncertainty. The derived slopes depends on whether there is a retro-reflected probe beam. The difference, perhaps a result of the laser cooling effect, was also noted in Ref. [7]. Taking into account that the detected laser power has a typical relative uncertainty of about 1%, combined with the slopes determined in Fig.4, we can estimate that the uncertainty due to laser power should be less than 0.1 kHz.

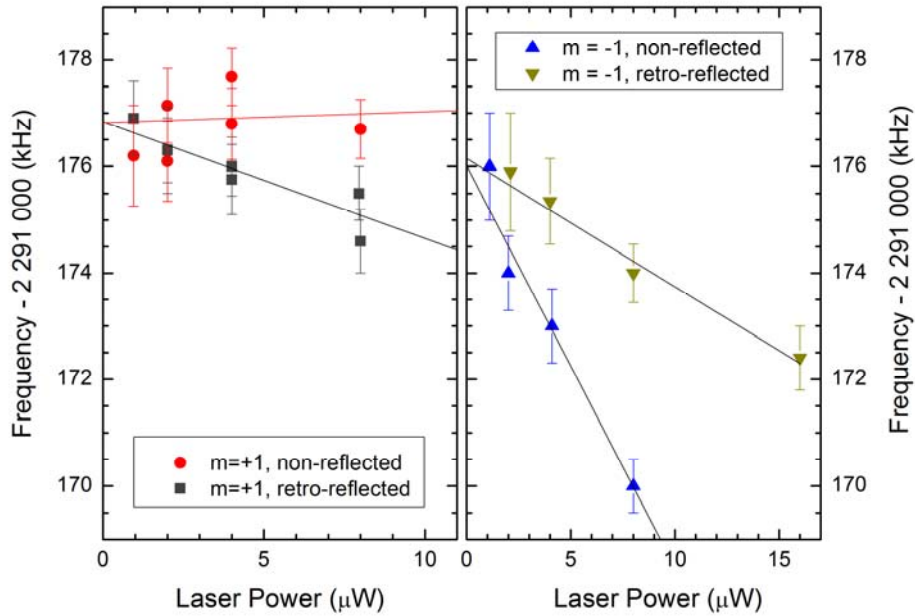


Fig.4 (Color online) Dependence of the measured frequency interval on the probe laser power.

Zeeman Shift: The first-order Zeeman shift is cancelled for the 2^3P_1 - 2^3P_2 interval [7]; only the second-order effect contributes to shifts, which can be precisely calculated at a given magnetic field [20]. In this work, a bias magnetic field of 10-20Gauss is applied. The measured values along with the calculated Zeeman shifts are shown in Fig.5. The bias B field was determined by measuring the frequency interval between the two transitions: $2^3P_1 (m=-1) \leftarrow 2^3S_1 (m=0)$ and $2^3P_1 (m=1) \leftarrow 2^3S_1 (m=0)$ with an accuracy of better than 5mG. The

resulted contribution to the uncertainty in the final determined ν_{12} value should be less than 0.09 kHz. The contribution due to residue, un-shielded magnetic field ($<0.5\text{mG}$) in the probing region is below 10 Hz.

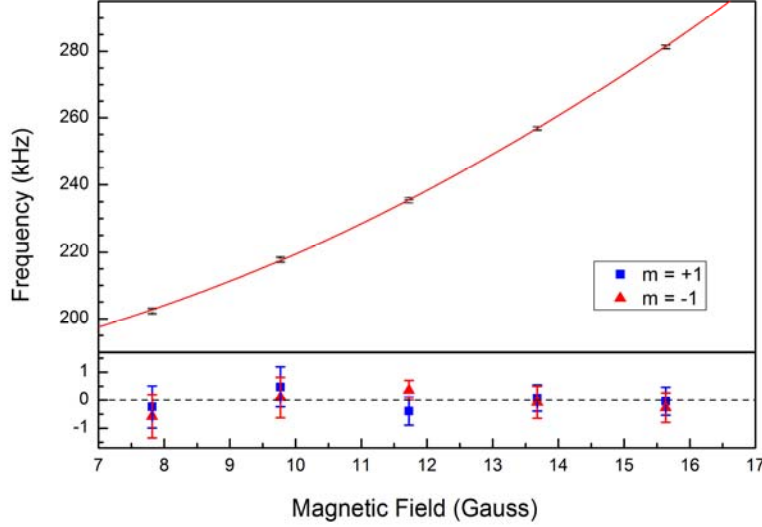


Fig.5 (Color online) The $2^3P_2-2^3P_1$ splitting obtained at different magnetic fields. The dots are the measured values and the solid curve is for the calculated second-order Zeeman shifts. The differences are given in the lower panel. The squares and triangles present for the transitions measured using σ^+ ($m = +1$) and σ^- ($m = -1$) circularly polarized laser beams, respectively.

Quantum Interference: A systematic shift arises from the quantum interference among the 2^3P_J states [21]. Recently a systematic effect due to interference from distant neighboring resonances have been fully developed [21-24]. According to the calculations by Marsman *et al.* [15], the quantum interference shift is inversely proportional to the frequency difference between the levels. Despite a frequency difference of 2.3 GHz between the 2^3P_1 and 2^3P_2 levels, which is over 1400 times of the natural width of the $2^3P \leftarrow 2^3S$ transition, the induced shift on the frequency interval could be at the level of kHz, and therefore must be taking into account. This effect was overlooked in the community and was not included in the result given by Shiner's group in North Texas.[7] Later, a correction of 1.2 ± 0.1 kHz was proposed [15] on the original value to yield a new value of $2\,291\,177.1 \pm 1.0\text{kHz}$.

Following the recipe given in Ref. [15], we calculated that the corresponding correction to the measured interval is 1.21 ± 0.16 kHz according to the experimental conditions in the present study. Because we sampled the whole spectrum using a total of 44 points with a frequency interval of 0.3 MHz near the line centers (see Fig.3) and the line centers were determined from fitting of the spectral profiles, the correction is independent to either the starting frequency or the frequency interval of the scan. This was not the case in Refs. [15, 22], where only four points were used to determine a line center.

Doppler Shift: A “cat’s eye” reflection configuration is used to align the probe beam. Deviation in the alignment is determined to be less than 20 μrad , which corresponds to a Doppler shift of less than 20 kHz in each transition, $2^3\text{P}_2 \leftarrow 2^3\text{S}_1$ or $2^3\text{P}_1 \leftarrow 2^3\text{S}_1$. In order to investigate the possible effects on the frequency interval due to residual Doppler shifts, we purposely misaligned the probing laser beam, which led to a Doppler shift of about 100 kHz in each observed transition frequency. As shown in Fig. 6(a), despite the large shift in each transition, no change in the frequency difference between the two transitions is detected. Therefore, we estimate that the deviation in the derived frequency interval due to the Doppler shift should be less than 0.11 kHz.

Polarization: The probing laser beam is linearly polarized with its polarization direction in parallel to the bias magnetic field. We also investigated the deviation due to imperfect alignment by purposely misaligning the polarization (Fig. 6(b)). No effect on the measured interval was observed even under a considerably large misalignment of 20° .

Amplitude Modulation: The spectral scan was conducted by tuning the frequency of the first-order sideband produced by the fiber EOM. The relative intensity of the sideband is controlled by the amplitude of the electrical field applied on the EOM according to the

first-order Bessel function: $J_1^2(\beta)$, where $\beta = \frac{\pi V^2}{2V_{1/2}^2}$, V is the RF voltage applied on the crystal

and $V_{1/2}$ is the half wave voltage of the EOM crystal. The relative intensity of the first-order sideband is kept at $J_1^2(\beta) = 34\%$. At this value, the Bessel function has a vanished first-order dependence on V , and the residual deviation on ν_{12} is expected to be less than 10 Hz. We verified that by applying different RF power (therefore different relative intensity of the sideband). As shown in Fig.6(c), the deviation on ν_{12} due to this effect is negligible under the conditions of our measurements.

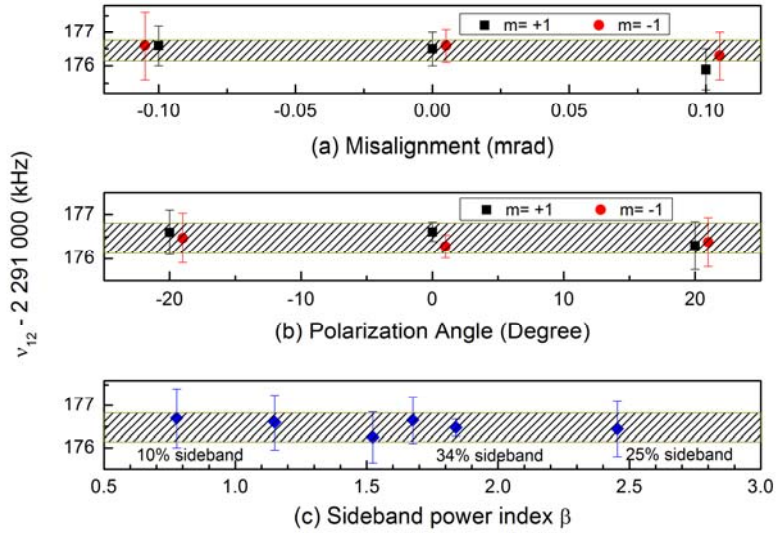


Fig.6 (Color online) Investigation of systematic deviations due to (a) Doppler shift, (b) misalignment of the laser polarization, (c) RF power (normalized) applied on the EOM to produce sidebands on the probe laser.

Other Systematic Effects: We have also investigated other factors which may potentially introduce systematic deviations in the result, including: (i) AC Stark shift due to scattering light, either from the strong laser beams used for transvers-cooling, or from the pump laser; (ii) The RF field used to drive the discharge may also affect the atoms in the probing region; (iii) Non-uniform distribution of the atomic beam, the laser beam, and the magnetic field. We verified the results by deliberately changing the power of the transvers-cooling laser beam, RF discharge source, and of the pumping laser. We also did the same measurements by preparing the metastable atoms (2^3S_1) at different sub-magnetic levels ($m = -1$ or $m = +1$) and by reversing the polarization of the probing laser and the magnetic field to check the consistency. As shown in Fig.7, all the results agree within the stated uncertainty of the present study. Note that two narrow (0.5 mm) slits, with a distance of 2 m, were used to collimate the atomic beam. We did not observe any influence due to non-uniform distribution of the atomic beam or the magnetic field by repeating the measurements using slightly different slit positions. The contribution from above factors is estimated to be less than 0.19 kHz.

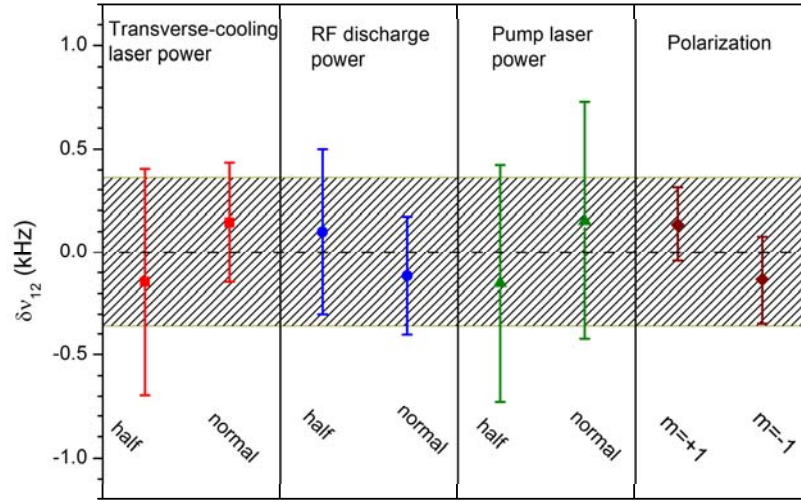


Fig.7 (Color online) Investigation on the potential systematic deviations

Table1 Uncertainty budget (in kHz)

Source	ν	$\Delta\nu(1\sigma)$
Statistical	2 291 176.48	0.17
Zeeman Effect		0.09
Laser power		0.10
Laser polarization		0.08
1st-Order Doppler		0.11
Others		0.19
Quantum interference	+1.21	0.16
Total	2 291 177.69	0.36

The uncertainty budget is given in Table 1. In total, 15419 scans were included and the resulted statistical uncertainty has been reduced to 0.17 kHz. Taking into account the corrections and systematic uncertainties, we obtained a result for the ν_{12} value as $2\,291\,177.69 \pm 0.36$ kHz. The value is consistent (0.16 ± 0.51 kHz) with the most recent microwave study (York '09) [12] which has a similar precision, and also agrees (0.5 ± 1.0 kHz) with the previous laser spectroscopy in an atomic beam (North Texas '00) [7] after correction of quantum interference [15], but deviates (2.0 ± 0.6 kHz) from that of saturation spectroscopy (Harvard '05) [11]. The present value also agrees with the most recent theoretical result

taking into account all QED effects up to the order of $\alpha^5\text{Ry}$ (Pachucki '10) [3]. The difference between the experimental and theoretical results is $-1.2 \pm 0.4_{\text{exp}} \pm 1.7_{\text{theo}}$ kHz. It indicates that the experimental results (both York '09 and this work) are sensitive to the $\alpha^6\text{Ry}$ terms which have never been calculated. Further improvements on the experimental accuracy and theoretical investigations on the high-order QED effects can be used to check the consistency of QED with an increased precision and to determine the fine-structure constant.

The authors thank Dr. Wei Jiang and Dr. Zheng-Tian Lu from Argonne National Laboratory, and Zong-Chao Yan from University of New Brunswick for helpful discussions, and for comments on the manuscript. This work is jointly supported by NSFC (11304303, 91221304 & 21225314), CPSF (2013M541828), CAS (XDB01020000) and FRFCU.

References:

- [1] T. Zhang, Z. C. Yan, and G. W. F. Drake, Phys. Rev. Lett. **77**, 1715 (1996).
- [2] K. Pachucki and V. A. Yerokhin, Phys. Rev. A **80**, 019902(E) (2009).
- [3] K. Pachucki and V. A. Yerokhin, Phys. Rev. Lett. **104**, 070403 (2010).
- [4] C. Schwartz, Phys. Rev. **134**, A1181 (1964).
- [5] S. M. Hu, Z. T. Lu, and Z. C. Yan, Front Phys. China **4**, 165 (2009).
- [6] G. W. F. Drake, Can. J. Phys. **80**, 1195 (2002).
- [7] J. Castilleja, D. Livingston, A. Sanders, and D. Shiner, Phys. Rev. Lett. **84**, 4321 (2000).
- [8] C. H. Storry, M. C. George, and E. A. Hessels, Phys. Rev. Lett. **84**, 3274 (2000).
- [9] M. C. George, L. D. Lombardi, and E. A. Hessels, Phys. Rev. Lett. **87**, 173002 (2001).
- [10] G. Giusfredi, P. C. Pastor, P. De Natale, D. Mazzotti, C. de Mauro, L. Fallani, G. Hagel, V. Krachmalnicoff, and M. Inguscio, Can. J. Phys. **83**, 301 (2005).
- [11] T. Zelevinsky, D. Farkas, and G. Gabrielse, Phys. Rev. Lett. **95**, 203001 (2005).
- [12] J. S. Borbely, M. C. George, L. D. Lombardi, M. Weel, D. W. Fitzakerley, and E. A. Hessels, Phys. Rev. A **79**, 060503 (2009).
- [13] M. Smiciklas and D. Shiner, Phys. Rev. Lett. **105**, 123001 (2010).
- [14] K. Pachucki, Phys. Rev. Lett. **97**, 013002 (2006).
- [15] A. Marsman, M. Horbatsch, and E. A. Hessels, Phys. Rev. A **86**, 040501 (2012).
- [16] C. Y. Chen, K. Bailey, Y. M. Li, T. P. O'Connor, Z. T. Lu, X. Du, L. Young, and G. Winkler, Rev. Sci. Instrum. **72**, 271 (2001).
- [17] C. F. Cheng, W. Jiang, G. M. Yang, Y. R. Sun, H. Pan, Y. Gao, A. W. Liu, and S. M. Hu, Rev. Sci. Instrum. **81**, 123106 (2010).

- [18] J. Alnis, A. Matveev, N. Kolachevsky, T. Udem, and T. W. Hansch, Phys. Rev. A **77**, 053809 (2008).
- [19] C. F. Cheng, Y. R. Sun, H. Pan, Y. Lu, X. F. Li, J. Wang, A. W. Liu, and S. M. Hu, Opt. Expr. **20**, 009956 (2012).
- [20] Z. C. Yan and G. W. F. Drake, Phys. Rev. A **50**, R1980 (1994).
- [21] M. Horbatsch and E. A. Hessels, Phys. Rev. A **82**, 052519 (2010).
- [22] M. Horbatsch and E. A. Hessels, Phys. Rev. A **84**, 032508 (2011).
- [23] A. Marsman, E. A. Hessels, and M. Horbatsch, Phys. Rev. A **89**, 043403 (2014).
- [24] D. C. Yost, A. Matveev, E. Peters, A. Beyer, T. W. Hänsch, and Th. Udem, Phys. Rev. A **90**, 012512 (2014)